Magnitude scaling of induced earthquakes

Benjamin Edwards, John Douglas

Magnitude Scaling of Induced Earthquakes

Benjamin Edwards[1*] *and John Douglas*[2]

[1] Swiss Seismological Service, ETH Zürich, Zürich, Switzerland.

[2] Seismic and Volcanic Risks Unit (RSV), Risks and Prevention Division (DRP), BRGM, Orléans, France.

[*] Corresponding Author -- email: edwards@sed.ethz.ch; address: Swiss Seismological Service, ETH Zürich, Sonneggstrasse 5, 8092 Zürich, Switzerland; telephone: +41 44 632 8963.

Abstract

Presented are the results of an earthquake magnitude homogenization exercise for several datasets of induced earthquakes. The result of this exercise is to show that homogeneous computation of earthquake moment- and local-magnitude is useful in hazard assessment of Enhanced Geothermal Systems (EGSs). Data include records from EGSs in Basel (Switzerland), Soultz (France) and Cooper Basin (Australia); natural geothermal fields in Geysers (California) and Hengill (Iceland), and a gas-field in Roswinkel (Netherlands). Published catalogue magnitudes are shown to differ widely with respect to M_w, with up to a unit of magnitude difference. We explore the scaling between maximum-amplitude and moment-related scales. We find that given a common magnitude definition for the respective types, the scaling between moment- and local-magnitude of small earthquakes follows a second-order polynomial, consistent with previous studies of natural seismicity. Using both the Southern-California M_L scale and a PGV-magnitude scale (M_{equiv}) determined in this study, we find that the datasets fall into two subsets with well-defined relation to M_w: Basel, Geysers and Hengill in one and Soultz and Roswinkel in another (Cooper Basin data were not considered for this part of the analysis because of the limited bandwidth of the instruments). M_{equiv} was shown to correlate 1:1 with M_L, albeit with region-specific offsets, while the distinct subsets in the M_{equiv} to M_W scaling led us to conclude that source and/or attenuation properties between the respective regions were different.

Keywords: Induced Seismicity; Earthquakes; Magnitude; Moment; Peak Ground Velocity; PGV; Attenuation; Amplification.

1 Introduction

Enhanced Geothermal Systems (EGSs) aim to provide sustainable, cost-effective and environmentally-friendly energy. They build upon the concepts of classic geothermal energy production, but facilitate the production in case of insufficient fluid conductivity. An EGS project aims to increase reservoir permeability through the use of micro-seismicity, with high-pressure fluids forced into the system creating new, or opening pre-existing fractures in the rock. Such methods provide the potential for initiating geothermal systems in any region with a sufficient temperature-gradient; however, the substantial cost of such projects means that both water-heating and electricity production are required to make them economically viable. The water-heating requirement implies that EGS projects are often set up in populated regions, since the transport of heated water requires costly insulation and transit pipelines. One such EGS project was the Deep Heat Mining Project in the city of Basel, Switzerland. The project aimed to provide up to 3MW of electricity, in addition to 20MW thermal energy, through a 200°C reservoir at 5km depth. Fluid injection was abruptly halted on the 8th December, 2006, after increasing seismicity culminated in a M_L 2.6 event. A few hours later a M_L 3.4 earthquake caused widespread light damage resulting in insurance claims of over $9M (Giardini, 2009).

A thorough risk assessment of an EGS project is clearly required in order to assess and mitigate potential losses and appease the local population. Given the induced seismicity related to an EGS, a key component of such a risk study is a seismic hazard assessment. Such hazard studies are typically carried out for sensitive facilities such as nuclear power stations. In these cases, events with magnitudes between M_w 5.5 and 7.5 are typically the most important since they have the most impact on long return-period hazard (Bazzurro and Cornell, 1999). However, in the case of an EGS, magnitudes of interest start at around M_w 2 due to the proximity to populated areas and the goal of avoiding nuisance to the population. In order to provide the frequencies of exceeding given ground-motion (intensity) measures within particular intervals, probabilistic seismic hazard analysis (PSHA) integrates ground-motion estimates over the magnitude-occurrence probability distribution. This is

facilitated through statistical analysis of earthquake magnitude catalogues, where the a- and b-values of the Gutenberg and Richter (1944) Relation are defined for a given source area. Consistent earthquake magnitude is, therefore, a critical component of PSHA.

Seismic monitoring of an EGS typically involves several medium- or short-period velocimeters (sensors that measure ground velocity) around the reservoir. This facilitates hypocentre localisation, depending on the methods employed, to within several hundred to tens of metres. Magnitudes are typically provided based on peak-amplitude measures, with correction for the source-station distance. The most common scale is the local- or Richter-magnitude, M_L (Richter, 1935):

$$M_L = \log_{10} A + f(R), \quad (1)$$

with A the peak-amplitude (in mm) on a Wood-Anderson torsion seismometer and $f(R)$ a correction factor for attenuation over distance R. The main problem with such scales is that the agency-dependent application of the attenuation correction often results in significantly different magnitudes being assigned for the same size earthquake occurring in different regions (Fäh *et al.*, 2011). In PSHA, the moment magnitude is usually used, since: it does not saturate at large magnitudes (although this is obviously not an issue for small EGS shocks); it is mostly agency-independent due to the analysis of very-low frequency (hence weakly-attenuated or -amplified) signals and; leads to simple, and therefore robust, recurrence statistics (e.g., a- and b-values). Furthermore, the M_W scale is the only one that can be directly estimated from fault parameters (length, width and offset), typically used to assess the occurrence rate of large (infrequent) earthquakes. Nevertheless, in the case of induced seismicity, it still has to be shown that the M_W scale is appropriate for PSHA, since it is based on fault area and slip, and therefore correlated to low-frequency ground motions. In this study we construct a homogenized earthquake catalogue including moment, local and PGV-equivalent magnitudes for a range of induced events. For convenience we refer to the magnitudes calculated in this work as reference values, since we can assure a common procedure and scale. However, magnitudes are, to an extent, an arbitrary measure.

The catalogue magnitudes may include processing for which we cannot account, such as expert judgement. And indeed, the use of regional specific attenuation corrections may be necessary due to differences in the propagation media. This should nevertheless become apparent upon comparison of the different magnitudes.

2 Determination of Moment Magnitude

We follow the method of Edwards et al. (2010) for the computation of moment magnitudes for small earthquakes. The method is based on the far-field spectral model of Brune (1970, 1971) and was shown to provide magnitudes consistent within ±0.1 units of moment tensor (MT) solutions of M>3 events in Switzerland. MT solutions require waveform matching of long-period arrivals, which may not be possible for small events due to noise or band-limited instrumentation. In contrast, spectral matching to obtain moments only requires fitting of the flat portion of displacement spectra, which can be done at fairly high frequencies above the background noise for small events. Therefore, such methods are the only suitable approach to determine M_w for such earthquakes.

2.1 Data and Processing

Data were available from a range of instrument types depending on location. More information can be found in Douglas et al. (2013). All data were first corrected for the full instrument response to provide traces with units of ground velocity. Analysis windows were chosen based on a 5-95% square velocity integral around the peak velocity. The multi-taper Fast Fourier Transform (mtFFT) with 5-3π prolate tapers was used to convert these into Fourier velocity spectra, and a 1Hz log-average smoothing filter was applied. Noise windows were taken from the first 5s of the traces, and processed in the same way. To ensure we did not underestimate the noise, the resulting noise estimates were conservatively raised to ensure that they matched the analysis window amplitudes at the lowest and highest frequencies of the spectrum. Following this, the valid frequency limits (f_{min} and f_{max}) of the analysis spectra at three times the noise level were determined. To retain a spectrum, we required that this bandwidth (f_{max}/f_{min}) exceeded 10.

2.2 Model Setup

As in Edwards et al. (2010) we assumed a simple 1/R geometrical decay, while the anelastic attenuation (t^*) is determined on a path-specific basis during the inversion along with the spectral plateau (Ω_0) and the source corner-frequency (f_c). In the case of induced events recorded at short distances the attenuation terms should not be critical but the aim here is for consistency rather than precision. For instance, in the case of an increase in the decay exponent of 10% (e.g., $1/R^{1.1}$), the determined M_w would be 0.05 too low at 5km, or 0.07 too low at 10km when assuming 1/R decay. Site amplification, which is known to strongly vary from site-to-site, is difficult to quantify due to the lack of a reference. The inversion procedure detailed in Edwards et al. (2010) can account for site-specific amplification provided that either the average amplification across the network is known or at least one M_w value is independently available. When most stations are on hard rock, the average amplification can be set to unity, meaning that the resultant site-specific amplification is relative to the network average shear-wave velocity (V_s) profile (e.g., Poggi *et al.*, 2011). However, if strong site amplification exists the assumption of no average network amplification would cause M_w to be overestimated (as site amplification is mistakenly attributed to the source). We, therefore, adopted an approach to estimate the average network amplification through correlation of site effects. The κ_0 parameter (Anderson and Hough, 1984) characterises the high-frequency attenuation that is generally attributed to the upper layers of rock and soil beneath a site, and can be simply measured from the high-frequency decay of the Fourier acceleration spectra. Since it depends on properties of the site, κ_0 has been shown to correlate with the upper 30m time-travel average V_s (V_{s30}; e.g., Edwards *et al.*, 2011), which is itself known to correlate with site amplification (e.g., Borcherdt, 1994). Edwards et al. (2011) showed that, in Switzerland, the κ_0 could be used to approximate average amplification at a given site, A_j. However, such correlations are known to be associated with high uncertainty. In order to reduce this uncertainty, and increase the degree of freedom of the inversion for M_w, whilst still constraining the trade-off between amplification and magnitude, we

therefore fix the average amplification over the network (as opposed to individual station values). When lacking other information, we, can estimate this average network amplification, υ, using:

$$\log(\upsilon) = \frac{1}{N}\sum_{j=1}^{N}\left[1.31\log\left(\kappa_{0,j}\right) + 2.32\right] \quad (2)$$

with $\kappa_{0,j}$ equal to κ_0 at site j. The inversion for M_w was then constrained such that site-specific amplifications had to satisfy the average amplification, υ.

3 Comparison of Catalogue and Moment Magnitudes

In this section we compare the moment magnitudes estimating using the approach detailed above and the magnitudes listed in available catalogues for the six considered sites.

3.1 Basel, Switzerland

The Basel EGS project began fluid injection on 2nd December, 2006 and continued until the 8th when injection was halted due to rapidly increasing seismicity (Giardini, 2009). During this time around 11,570 m3 of water was injected at high pressures to stimulate the seismically active zone (Häring et al., 2008). Prior to shutdown water was being injected in excess of 50 l/s with wellhead pressures reaching up to 29.6 MPa (Häring et al., 2008, Deichmann and Giardini, 2009). Several hundred earthquakes directly related to the EGS were located during and after the injection phase (Deichmann and Giardini, 2009); however, we only analyse a subset that were manually located by the Swiss Seismological Service (SED). This subset comprises events larger than about M_w 1.3, and hence of most interest for seismic hazard, since they were possibly felt by the local population. In the case of this dataset, the majority of recordings were made on the sedimentary basin underlying the city of Basel on strong-motion surface sensors and borehole geophones deployed by Geothermal Explorers Ltd. Further recordings were available from the SED's broadband seismic network (SDSNet). Despite their limited quantity, the recordings on the SDSNet are particularly advantageous since Poggi et al. (2011) provide site-specific amplification (and a corresponding regional velocity model)

for these sites as part of a study of wider Swiss seismicity. As such, it was possible to constrain the inversion in terms of the trade-off between site amplification and magnitude by fixing the amplification at SDSNet sites.

In a previous comparison of magnitudes for earthquakes in the entire Swiss region, Goertz-Allmann et al. (2011) showed that:

$$M_W = 0.594M_L + 0.985 \pm 0.096 \qquad (M_L < 2)$$
$$M_W = 1.327 + 0.253M_L + 0.085M_L^2 \pm 0.079 \qquad (2 \leq M_L \leq 4) \quad (3)$$
$$M_W = M_L - 0.3 \pm 0.105 \qquad (M_L > 4).$$

This relation was shown to be very similar to another model of regional M_L:M_w scaling in Europe derived by Grünthal et al. (2009). When compared with M_L values from the Earthquake Catalogue of Switzerland (ECOS09), inverted M_w values computed here were found to conform, on average, to this M_W:M_L scaling relation (Figure 1). On closer analysis, ECOS09 M_W, which were estimated from M_L using the scaling relation in Equation (3), are generally higher than the directly inverted values, particularly for smaller events (Figure 1b). This is because site amplification was not taken into account in the case of M_W converted from M_L in ECOS09, whilst for the inverted M_w presented here, amplification was calculated for each recording site and is consistent with the Swiss reference velocity model of Poggi et al. (2011). Of interest is the impact of borehole installations on observed amplification. The deepest boreholes (adjacent to the injection well) are instrumented with three seismometers: OTTER, OTER1 and OTER2. These lie at the surface (298m above sea-level), 545m and 2785m below the surface respectively. Average amplification obtained for OTTER was a factor of 2.1, consistent with its position at the top of a sedimentary basin (with low seismic velocity V_{s30}=418ms^{-1}). Borehole sites OTER1 and OTER2 showed average amplification of 0.34 and 0.19 respectively. Part of this deamplification is expected due to the fact that there is no free-surface effect in the borehole (which is assumed to be a factor of 2 for all sites). Accounting for the lack of free surface at OTER1 and OTER2 leaves amplification of 0.68 and 0.38 respectively. The deamplification is accounted for

by considering that the rock velocity at the instrument location [OTTER1 $V_s \approx 2 kms^{-1}$ and OTER2 $V_s \approx 3.5 kms^{-1}$ (Bethmann *et al.*, 2012)] is higher than the reference rock with $V_{s30}=1.1 kms^{-1}$ (Edwards *et al.*, 2013). Since most of the EGS recordings are sited on deep sediments (more so for smaller events only recorded locally on the sedimentary basin), they consequently undergo significant amplification, computed magnitudes are higher when they do not properly account for this phenomenon (e.g., M_w converted from M_L in ECOS09). Nevertheless, the similarity of magnitude scaling between the EGS events studied here and those in the wider tectonic context indicate that there is nothing particularly special (e.g., in terms of radiated energy) about EGS events.

3.2 Geysers, California

The Geysers Geothermal Field is primarily a dry-steam field in a natural greywacke sandstone reservoir at around 1-3 km depth. Seismic activity has increased since commercial exploitation started in 1960 (Majer *et al.*, 2007). Local seismicity is monitored through the dense Berkeley-Geysers (BG) network, consisting of 29 3-component geophones, in addition to several nearby stations of the Northern California Seismic Network (NCSN). We analyse data from the BG network recorded between 2007 and 2011, made available by the Northern California Earthquake Data Center.

Several events in the dataset include independent M_w estimates from MT inversions using data recorded on broadband NCSN instruments. We use this to constrain the amplification-magnitude trade-off by fixing events with known $M_w \geq 3.5$. Five further events with $M_w < 3.5$ assigned by NCSN were available and their values are compared with those derived by us in Figure 2. Three of the five events are consistent to within 0.1 units. However, two of the events differ in magnitude by around 0.15. Whilst it is not unreasonable to expect our inverted values to differ by 0.15 units from the truth, given the known standard deviation of 0.1, the moment tensor solutions are also not definitive, particularly for such small magnitudes.

Comparing the remaining catalogue magnitudes with M_w we find that the duration magnitude (M_d) used by the Berkeley-Geysers (BG) network scales well with M_w (Figure 3), with $R^2 = 0.98$, but with a constant offset. Using an L2 minimization, assuming known M_d, we find that for the Geysers catalogue in the range $0.9 \leq M_d \leq 3$:

$$M_w = 0.90\mathrm{M_d} + 0.47 \pm 0.08 \quad (4)$$

Catalogue M_L values (although there are few in this case) tend to be slightly lower than M_w, opposite to the results for the Basel data in this magnitude range (Figure 3b).

The largest magnitude determined in our analysis was M_w 3.9. The offset of M_L versus M_w in Figure 3 suggests this is anonymously high. A corresponding value from the NCSN was not available. However, using the empirical GMPEs derived by Douglas et al. (2013) for induced seismicity we can see that a mean value of M_w 3.9 is consistent with recorded peak ground velocity (PGV) for this event. Similarly, upon recomputing M_L for this event we find a higher value of 4.4, which is then more consistent with the general trend.

3.3 Hengill, Iceland

Data from induced earthquakes related to the Hengill geothermal area were recorded as part of the I-GET FP6 project (Jousset *et al.*, 2011). The temporary array consisted of seven Guralp Systems broadband seismometers. The dataset was supplemented by recordings from three 5s Lennarz velocimeters of the Iceland Meteorological Office (IMO). Seismicity is thought to be related to cooling and subsequent contraction of the rock (Jousset *et al.*, 2011). κ_0 values were first measured for each station. From this the average amplification was estimated to be a factor of 2.1 using equation (2). Computed M_w values are shown in Figure 4, compared with catalogue values for local and moment magnitude from IMO. An offset of around 0.3 units between the M_w value determined here and the catalogue values is apparent. The inverted M_w values also fall above the M_L:M_w trend line of Goertz-Allmann et al. (2011). Such a systematic difference suggests that the magnitudes were computed using different assumptions. A particularly sensitive choice is the attenuation correction.

In our computation, we used the simplest assumption of 1/R decay; however, given adequate knowledge of local attenuation, this may have been assigned differently.

3.4 Roswinkel, Netherlands

Roswinkel is the location of a natural gas-field in north-east Netherlands. The gas field is situated at a depth of around 2 km and was exploited between 1980 and 2005. The strongest earthquake recorded was an M_L 3.4 event, which led to shaking equivalent to macroseismic intensity VI. Our dataset consists of 27 events with $0.9 \leq M_L \leq 3.2$ recorded by up to five strong-motion sensors deployed to record the seismicity related to the gas-field. Of these, 24 were assigned M_w values. Unfortunately, most events were well recorded by only one to three instruments which may lead to large deviations in magnitude estimation due to radiation effects. Nevertheless, the plot of M_w versus catalogue M_L shows a surprisingly linear scaling, with minimal scatter (Figure 5). Additionally, the magnitudes conform quite closely to the Swiss M_w:M_L scaling relation of Goertz-Allmann et al. (2011), with a constant offset of around 0.1 units.

3.5 Soultz, France

The Soultz dataset is from a research EGS project situated in the Rhine Graben. Data are obtained from three velocimeters, which recorded numerous earthquakes induced over the course of several reservoir stimulation phases between 2003 and 2010. The main reservoir is located at around 5km depth and is at approximately 200°C. We analyse data from the 2003 injection phase. From the measured κ of 0.03s, it was estimated using Equation (2) that the average amplification would be a factor of 2.1. The inversion showed that amplification was similar at all three instrumentation sites (2.6, 1.8 and 2.0), probably due to their close proximity on similar geology. A comparison of catalogue M_L (provided by l'École et Observatoire des Sciences de la Terre, EOST) versus inverted M_W values is shown in Figure 6. In this case, the catalogue M_L values are generally higher than M_W, and deviate by over 0.5 units from the Swiss M_w:M_L scaling relation. One explanation for this could be related to the very short recording distances for this data. In this case, the correct calibration of the

M_L scale at such distance is critical, and may be overlooked if regional seismicity was used for its derivation.

3.6 Cooper Basin, Australia

Cooper Basin lies in central Australia and is home to significant oil and gas production. A recent EGS experiment in 2003 was performed by injecting more than 20,000 m^3 of water into the Granitic crust at 4.25 km depth (Baisch *et al.*, 2006). Thousands of induced events were detected and recorded by an eight station three-component geophone network deployed in boreholes at depths between 70 and 1700 m (Baisch *et al.*, 2006). The limited instrument sensitivity presents a challenge in this case; with the corner-frequency of the instrument's velocity-response at around 10Hz. Nevertheless, due to the relatively low-attenuation (recordings at short distance), and small magnitude, the spectral-plateaus could still be reliably measured. M_w could, therefore, still be determined despite the strongly band-limited data. Attenuation was measured as between κ=0.02 and 0.04s, which is not particularly low, despite the borehole installations. This is probably because, despite the sensors being located in boreholes, the limited penetration depths did not exceed the limit of the sedimentary basin. Based on the observed attenuation, average amplification was estimated to be a factor of 2.3. Inverted values were consistent with borehole depths: the shallower boreholes (90-110m) generally leading to higher recorded amplification than the deeper boreholes (220-450m), with factors of 3.6 and 1.1 respectively. In this case, we also accounted for the fact that the borehole sensors are not subject to the free-surface effect (roughly a factor of two). The computed M_w (Figure 7) are systematically lower than M_w and lie above the Swiss M_L:M_w relation by about 0.3 units. The largest event in our database had M_L 2.5, and was assigned as M_w 2.9. In this case, we suspect that the significantly band-limited instrument led to the underestimation of M_L.

4 Common Local Magnitude and M_{equiv}

In the previous section, we compared catalogue magnitudes with computed M_w. Significant and systematic variations could be seen across the different datasets. This obviously has an impact on

the estimated hazard if a single ground motion prediction equation (GMPE) is used in all cases. An important question to pose is: whether such differences are really justified, or whether they arise purely from processing and computational decisions? In order to make a meaningful comparison between the datasets, we recomputed all M_L using a common correction for attenuation. This makes a similar assumption to that used for our M_w calculation: regional differences in attenuation have a low influence for short propagation distances. The equation used was as Equation (1), with *A* the displacement in mm on a Wood-Anderson Torsion Seismometer (here simulated), along with the attenuation correction used by the Southern California Seismic Network:

$$f(R) = -\log[0.3173\exp(-0.00505\mathrm{R})\mathrm{R}^{-1.14}] \quad (5)$$

which is modified from Kanamori et al. (1993) . The resulting comparison with M_w is shown in Figure 8. Two subsets are apparent: those events which follow the model of Goertz-Allmann et al. (2011): Geysers, Hengill and Basel (Figure 8a); and those which follow the same trend, but offset by around half a magnitude unit: Roswinkel and Soultz (Figure 8b). Interestingly, Roswinkel has shifted from presenting positive M_w-M_L residuals, to negative, highlighting that magnitudes are not absolute.

Edwards et al. (2010) and Deichmann (2006) showed, through numerical simulations, that differences in frequency dependent attenuation (e.g., Q and κ) have the most impact in scaling between M_L and M_w at low magnitudes, since, despite differences in stress-parameter, such events all have significant proportions of high-frequency energy at the source. As such, we would suspect that the two subsets of events exhibiting similar scaling behaviour undergo similar attenuation. Between the two, we could then infer that attenuation at Geysers, Hengill and Basel is higher than at Roswinkel (relative to the correction applied using Equation (5)). However, a further problem is apparent, and that is the non-uniform distance distribution between individual databases. Unfortunately, this could reflect discrepancies or bias in the distance-attenuation correction. For instance, Roswinkel and Soultz (comprising one of the subsets) have very short average distances of about 3 and 5km, respectively.

Bommer et al. (2006) introduced the concept of a PGV-referenced magnitude as part of their traffic-light alert system for EGS projects, using the example of Berlin, El Salvador. The PGV-equivalent magnitude (M_{equiv}), for a reference hypocentral depth was defined to be the event magnitude required for an event at that depth to produce the same surface PGV, according to a prescribed attenuation equation. In order to define the attenuation equation, we regressed M_w (to estimate M_{equiv}), PGV and hypocentral distance using an equation of the form:

$$\mathrm{M_{equiv}} = \mathrm{c_1} + \log(\mathrm{PGV}) + \mathrm{c_2}\log(\sqrt{\mathrm{R}^2 + \mathrm{c_3}^2}) \quad (6)$$

with R the hypocentral distance, and PGV in ms^{-1}. All datasets with the exception of Cooper Basin (because of the limited bandwidth of its data) were included in the regression. We found that $\mathbf{c_1} = 3.9720$; $\mathbf{c_2} = 2.1577$ and $\mathbf{c_3} = 4.6403$, with $\boldsymbol{\sigma_M} = 0.82$. Unfortunately, the rather large $\boldsymbol{\sigma_M}$ indicates that there is limited correspondence between M_w and PGV, at least using the functional form adopted. This may be due to the role of source properties (such as slip kinematics or stress-drop), which do not affect M_w, but have a significant impact on recorded PGV, particularly in the case of weakly attenuated signals. Whilst the minimisation aimed to reduce the misfit between moment and PGV-equivalent magnitude, PGV is nevertheless a point-measure on a seismogram. Therefore, it is not surprising that it behaves similarly to M_L, another point- and band-limited measure, as shown in Figure 9. This similarity in scaling can be seen in Figure 10, which shows M_{equiv} versus recalculated M_L. It can again be noticed that the data fall into the same two distinct subgroups.

Since in this case, the attenuation correction was specifically designed for the data (as opposed to the correction adopted for Southern California in the case of M_L). We can infer (after checking the residuals of the regression) that it is not a result of any bias in the distance correction which leads to the difference in M_L:M_w scaling. Rather, the difference must be a result of either: (a) different attenuation, or (b) different source properties in the different regions, or indeed, a combination of both.

5 Conclusion

We computed moment magnitude for induced earthquakes from a number of regions. Comparing these against catalogue magnitudes, we found that they all broadly follow similar scaling behaviour, but offset relative to one another. This scaling behaviour was found to follow a segmented polynomial curve, consistent with the results of Goertz-Allmann et al. (2011). The scatter of all catalogue M_L values versus M_w was significant, which leads us to question what reported earthquake magnitudes really tell us, and how they can be used in hazard assessments?

Part of the problem is through agency specific calibration of the M_L scale, for example, how attenuation is accounted for. This was highlighted by Fäh et al. (2011) during a catalogue homogenization for the Earthquake Catalogue of Switzerland 2009: events occurring in the border regions of Switzerland would be assigned systematically different magnitudes by the seismological observatories operating on either side of the border. Clearly, some differences in attenuation corrections may be justified. However, in order to compare all events independently of source agency, we recomputed the M_L values using a Californian attenuation model. In this case, with the same data used for the computation of M_L and M_w, and a unique attenuation correction, the scatter in the scaling plots was significantly reduced. Nevertheless, two sub-classes of events were apparent, the first with scaling exactly following the model of Goertz-Allmann et al. (2011), and a second with approximately a half unit offset. This observation itself may indicate that the two sub-groups require different attenuation corrections or calibration of the computation of M_L from Wood-Anderson amplitudes. Edwards et al. (2010) showed through simulated seismograms that the curvature of M_L:M_W scaling is strongly controlled by source scaling (i.e., how stress-drop varies with M_w). The similarity in shape of the M_L:M_W scaling in both subgroups indicates that average source-scaling is therefore similar in all regions.

What is important to note is that due to the control of M_L by relatively high frequencies (compared to M_w), it is more sensitive to differences in attenuation. This fact, and the resultant ambiguity in the

meaning of M_L, leads us to suggest that it is not suitable for ground-motion prediction or PSHA where components (GMPEs, recurrence statistics, etc.) are adopted from other regions. Similarly, we do not recommend that M_w is estimated from M_L, apart from in the case that the conversion equation is robustly determined from local (network specific) data (e.g., Douglas *et al.*, 2013). The magnitudes from the Cooper basin data were not included in this analysis, as we could not be sure that the significantly-limited instrument bandwidth (f>10Hz) did not have an adverse impact on estimated M_L. This highlights the importance of monitoring decisions: while low-cost geophones are suitable for detection and location, magnitude estimation requires recording in a suitable frequency bandwidth.

Finally, we computed a PGV-equivalent magnitude, M_{equiv}, using an attenuation model computed using the data of this study. It was shown that M_L and M_{equiv} scale 1:1, although offsets are apparent within particular datasets. This suggests a systematic difference in the PGV of records from a certain dataset, with respect to the Wood-Anderson response, and may be indicative of underlying source- or attenuation processes. Due to the 1:1 scaling of M_L and M_{equiv}, the scaling of M_w with M_{equiv} was similar to that observed for M_L: with two distinct sub-classes. Since the attenuation correction for PGV was computed using data from many regions, we could eliminate the influence of inappropriate distance correction interacting with different average recording distances. As a result, we inferred that the ground motion recorded in the various regions (Geysers, Hengill and Basel versus Soultz and Roswinkel) is fundamentally different, either due to different source-, and/or different regional attenuation-processes.

In the case of a probabilistic or deterministic hazard analysis for an EGS project, the expected earthquake magnitude distribution is required as an input. We have seen here, that if all M_L values are taken as equal, it would have a significant impact on the hazard calculated in different regions. In fact, after recomputing M_L we saw that differences with respect to our reference M_w were quite limited. The important aspect to consider is the compatibility of the magnitude computation (and

resulting distribution), the GMPE to be used in the hazard analysis and the observed data. What must be avoided, is for equations to be chosen ad-hoc (e.g., M_L attenuation corrections, or conversion from M_L to M_w), without consideration of the propagation of errors due to such decisions further down the line. Finally, we recommend that magnitudes are properly defined, and that they are calibrated with a suitable GMPE (e.g., Douglas *et al.*, 2013), such that in the case of hazard analysis, correct spectral ordinates can be properly estimated.

Acknowledgements

This study was partially funded by GEISER (Geothermal Engineering Integrating Mitigation of Induced Seismicity in Reservoirs) project funded under contract 241321 of the EC-Research Seventh Framework Programme (FP7). We thank Philippe Jousset for providing the data from Hengill; Michel Frogneux for the data from Soultz; Lawrence Berkeley National Laboratory Geysers/Calpine seismic network and NCEDC for the data from The Geysers; KNMI for the data from Roswinkel; the Swiss Seismological Service and Geothermal Explorers Ltd. for the data from Basel and Geodynamics Ltd. (Australia) for the data from Cooper Basin. We thank Lawrence Hutchings and Ernest Majer for their reviews, which led to improvements to the clarity of this article.

References

Anderson, J. G. and S. E. Hough (1984). A Model for the Shape of the Fourier Amplitude Spectrum of Acceleration at High-Frequencies, *Bulletin of the Seismological Society of America* **74**, 1969-1993.

Baisch, S., R. Weidler, R. Voros, D. Wyborn and L. de Graaf (2006). Induced seismicity during the stimulation of a geothermal HFR reservoir in the Cooper Basin, Australia, *Bulletin of the Seismological Society of America* **96**, 2242-2256.

Bazzurro, P. and C. A. Cornell (1999). Disaggregation of seismic hazard, *Bulletin of the Seismological Society of America* **89**, 501-520.

Bethmann, F., N. Deichmann and P. M. Mai (2012). Seismic wave attenuation from borehole and surface records in the top 2.5 km beneath the city of Basel, Switzerland, *Geophysical Journal International* **190**, 1257-1270.

Bommer, J. J., S. Oates, J. M. Cepeda, C. Lindholm, J. Bird, R. Torres, G. Marroquin and J. Rivas (2006). Control of hazard due to seismicity induced by a hot fractured rock geothermal project, *Engineering Geology* **83**, 287-306.

Borcherdt, R. D. (1994). Estimates of site-dependent response spectra for design (methodology and justification), *Earthquake Spectra* **10**, 617-617.

Brune, J. N. (1970). Tectonic Stress and Spectra of Seismic Shear Waves from Earthquakes, *Journal of Geophysical Research* **75**, 4997-&.

Brune, J. N. (1971). Correction, *Journal of Geophysical Research* **76**, 5002-&.

Deichmann, N. (2006). Local magnitude, a moment revisited, *Bulletin of the Seismological Society of America* **96**, 1267-1277.

Deichmann, N. and D. Giardini (2009). Earthquakes Induced by the Stimulation of an Enhanced Geothermal System below Basel (Switzerland), *Seismological Research Letters* **80**, 784-798.

Douglas, J., B. Edwards, B. M. Cabrera, V. Convertito, A. Tramelli, D. Kraaijpoel, N. Maercklin, N. Sharma and G. De Natale (2013). Predicting ground motion from induced earthquakes in geothermal areas, *Bulletin of the Seismological Society of America* **103**.

Edwards, B., B. Allmann, D. Fäh and J. Clinton (2010). Automatic computation of moment magnitudes for small earthquakes and the scaling of local to moment magnitude, *Geophysical Journal International* **183**, 407-420.

Edwards, B., D. Fäh and D. Giardini (2011). Attenuation of seismic shear wave energy in Switzerland, *Geophysical Journal International* **185**, 967-984.

Edwards, B., C. Michel, V. Poggi and F. D. (2013). Determination of Site Amplification from Regional Seismicity: Application to the Swiss National Seismic Networks. Accepted for publication in Seismological Research Letters.

Fäh, D., D. Giardini, P. Kästli, N. Deichmann, M. Gisler, G. Schwarz-Zanetti, S. Alvarez-Rubio, S. Sellami, B. Edwards and B. Allmann (2011). ECOS-09 Earthquake Catalogue of Switzerland Release 2011 Report and Database. Public catalogue, 17. 4. 2011. Swiss Seismological Service ETH ZurichReport SED/RISK.

Giardini, D. (2009). Geothermal quake risks must be faced, *Nature* **462**, 848-849.

Goertz-Allmann, B. P., B. Edwards, F. Bethmann, N. Deichmann, J. Clinton, D. Fah and D. Giardini (2011). A New Empirical Magnitude Scaling Relation for Switzerland, *Bulletin of the Seismological Society of America* **101**, 3088-3095.

Grünthal, G., R. Wahlstrom and D. Stromeyer (2009). The unified catalogue of earthquakes in central, northern, and northwestern Europe (CENEC)-updated and expanded to the last millennium, *Journal of Seismology* **13**, 517-541.

Gutenberg, B. and C. F. Richter (1944). Frequency of earthquakes in California, *Bulletin of the Seismological Society of America* **34**, 185-188.

Häring, M. O., U. Schanz, F. Ladner and B. C. Dyer (2008). Characterisation of the Basel 1 enhanced geothermal system, *Geothermics* **37**, 469-495.

Jousset, P., C. Haberland, K. Bauer and K. Arnason (2011). Hengill geothermal volcanic complex (Iceland) characterized by integrated geophysical observations, *Geothermics* **40**, 1-24.

Kanamori, H., J. Mori, E. Hauksson, T. H. Heaton, L. K. Hutton and L. M. Jones (1993). Determination of earthquake energy release and ML using TERRAscope, *Bulletin of the Seismological Society of America* **83**, 330-346.

Majer, E. L., R. Baria, M. Stark, S. Oates, J. Bommer, B. Smith and H. Asanuma (2007). Induced seismicity associated with enhanced geothermal systems, *Geothermics* **36**, 185-222.

Poggi, V., B. Edwards and D. Fäh (2011). Derivation of a Reference Shear-Wave Velocity Model from Empirical Site Amplification, *Bulletin of the Seismological Society of America* **101**, 258-274.

Richter, C. F. (1935). An instrumental earthquake magnitude scale, *Bulletin of the Seismological Society of America* **25**, 1-32.

List of Figure Captions

Figure 1: Comparison of moment magnitude (M_w) versus (a) local magnitude (M_L) and (b) Earthquake catalogue of Switzerland 2009 (ECOS09) M_w for the Basel EGS dataset. The Swiss M_L:M_w scaling relation of Goertz-Allmann et al. (2011) is shown.

Figure 2: Comparison between inverted and catalogue M_w values for Geysers, showing those events with fixed M_w.

Figure 3: Comparison of moment magnitude (M_w) versus catalogue (a) duration magnitude (M_d) and (b) local magnitude (M_L) for the Geysers dataset.

Figure 4: Comparison of moment magnitude (M_w) versus catalogue (a) local magnitude (M_L) and (b) moment magnitude (M_w) for the Hengill dataset. The Swiss M_L:M_w model is that of Goertz-Allmann et al. (2011).

Figure 5: Comparison of moment magnitude (M_w) versus catalogue local magnitude (M_L) for the Roswinkel dataset. The Swiss M_L:M_w model is that of Goertz-Allmann et al. (2011).

Figure 6: Comparison of moment magnitude (M_w) versus catalogue local magnitude (M_L) for the Soultz dataset. The Swiss M_L:M_w model is that of Goertz-Allmann et al. (2011).

Figure 7: Comparison of moment magnitude (M_w) versus catalogue local magnitude (M_L) for the Cooper Basin dataset. The Swiss M_L:M_w model is that of Goertz-Allmann et al. (2011).

Figure 8: Comparison of common M_L scale versus inverted M_w for all datasets in the study. (a) Geysers, Hengill and Basel events, along with the Swiss M_L:M_w model of Goertz-Allmann et al. (2011). (b) Roswinkel and Soultz events plotted along with the Swiss M_L:M_w model offset by 0.5 units.

Figure 9: Comparison of common M_{equiv} versus inverted M_w for all datasets in the study. (a) Geysers, Hengill and Basel events. (b) Roswinkel and Soultz events.

Figure 10: Comparison of M_L using the Southern California attenuation, with M_{equiv}.

Figures

(a) (b)

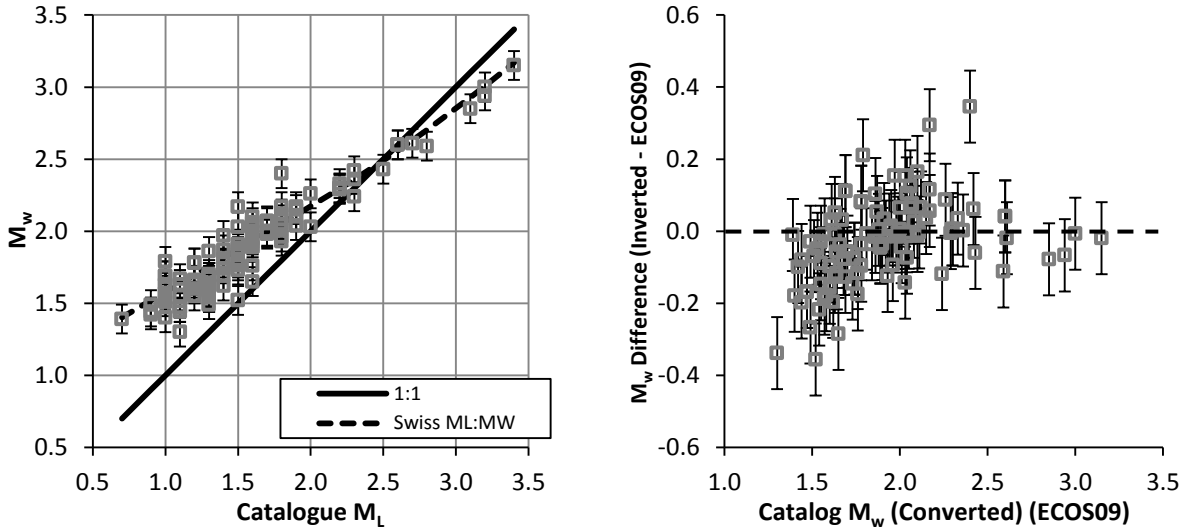

Figure 1: Comparison of moment magnitude (M_w) versus (a) local magnitude (M_L) and (b) Earthquake catalogue of Switzerland 2009 (ECOS09) M_w for the Basel EGS dataset. The Swiss M_L:M_w scaling relation of Goertz-Allmann et al. (2011) is shown.

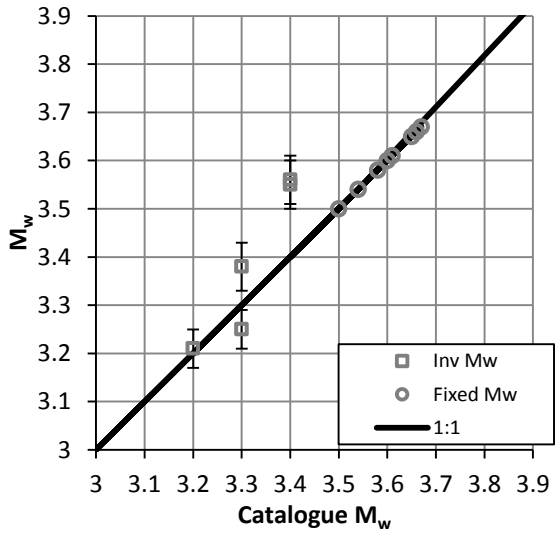

Figure 2: Comparison between inverted and catalogue M_w values for Geysers, showing those events with fixed M_w.

(a) (b)

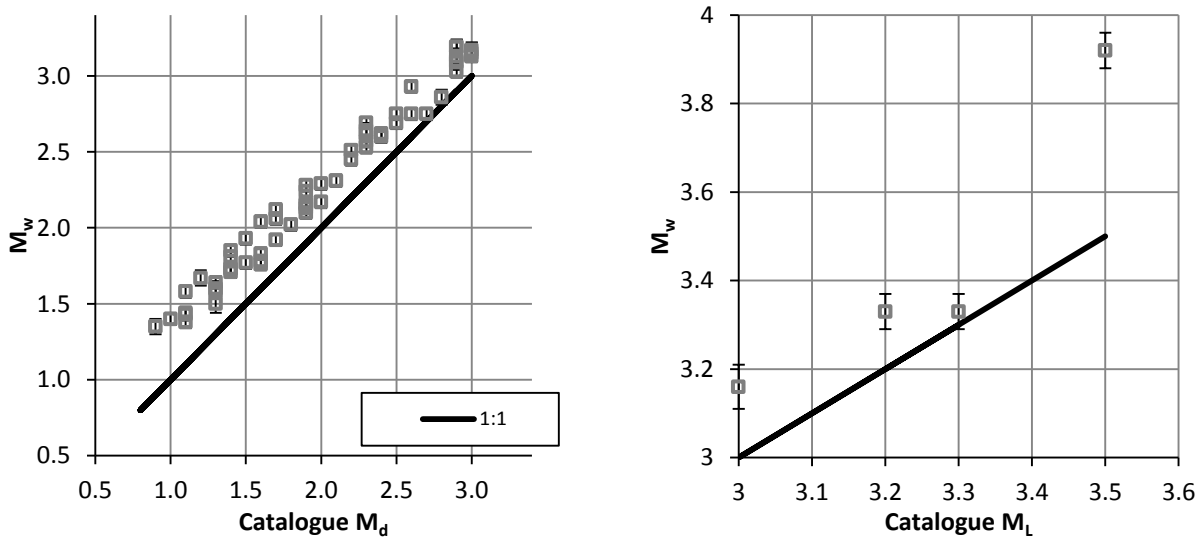

Figure 3: Comparison of moment magnitude (M_w) versus catalogue (a) duration magnitude (M_d) and (b) local magnitude (M_L) for the Geysers dataset.

(a) (b)

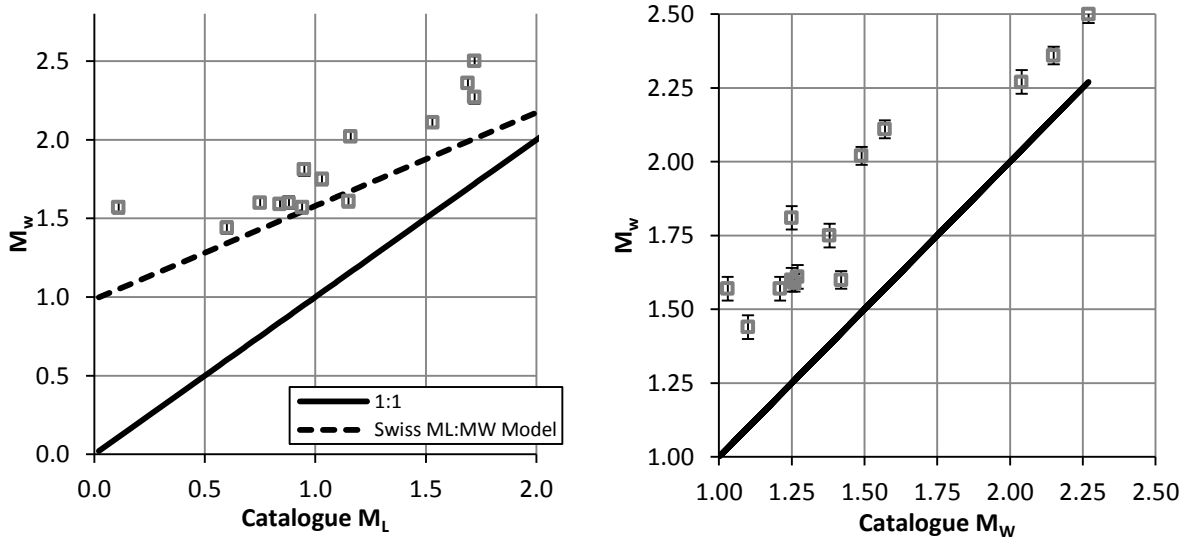

Figure 4: Comparison of moment magnitude (M_w) versus catalogue (a) local magnitude (M_L) and (b) moment magnitude (M_w) for the Hengill dataset. The Swiss M_L:M_w model is that of Goertz-Allmann et al. (2011).

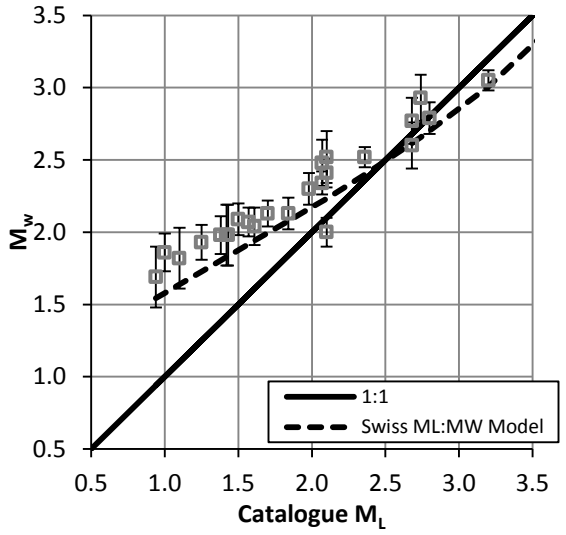

Figure 5: Comparison of moment magnitude (M_w) versus catalogue local magnitude (M_L) for the Roswinkel dataset. The Swiss M_L:M_w model is that of Goertz-Allmann et al. (2011).

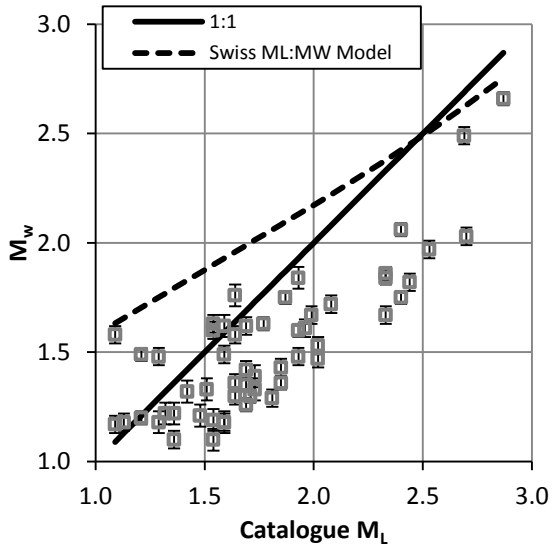

Figure 6: Comparison of moment magnitude (M_w) versus catalogue local magnitude (M_L) for the Soultz dataset. The Swiss M_L:M_w model is that of Goertz-Allmann et al. (2011).

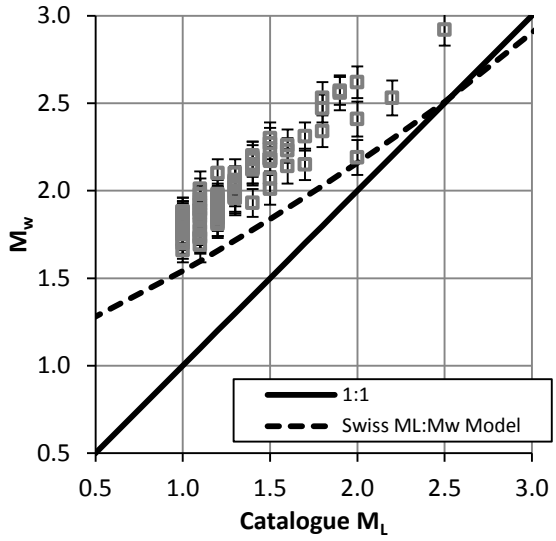

Figure 7: Comparison of moment magnitude (M_w) versus catalogue local magnitude (M_L) for the Cooper Basin dataset. The Swiss M_L:M_w model is that of Goertz-Allmann et al. (2011).

(a)

(b)

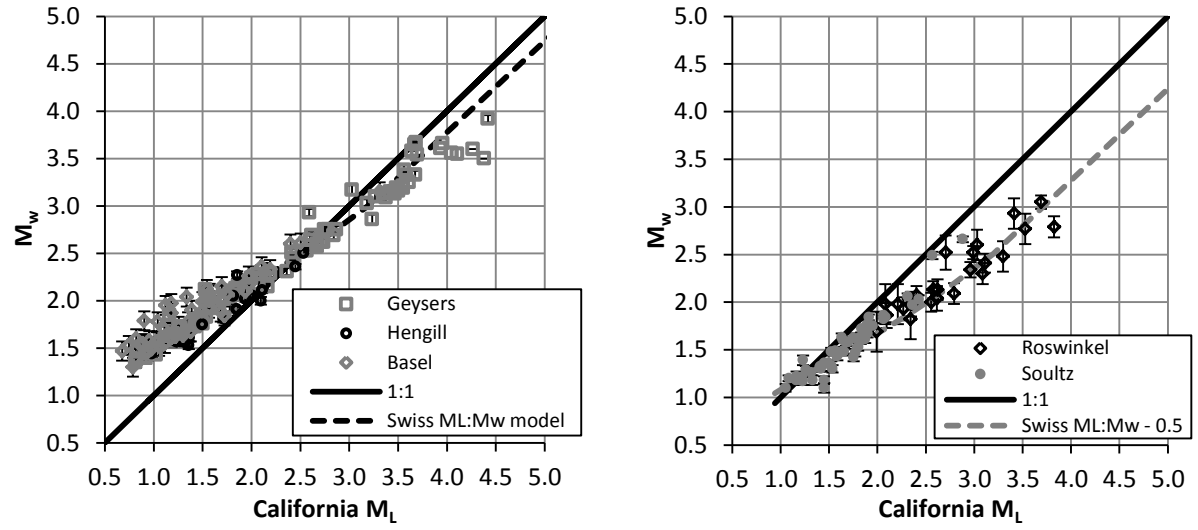

Figure 8: Comparison of common M_L scale versus inverted M_w for all datasets in the study. (a) Geysers, Hengill and Basel events, along with the Swiss M_L:M_w model of Goertz-Allmann et al. (2011). (b) Roswinkel and Soultz events plotted along with the Swiss M_L:M_w model offset by 0.5 units.

(a) (b)

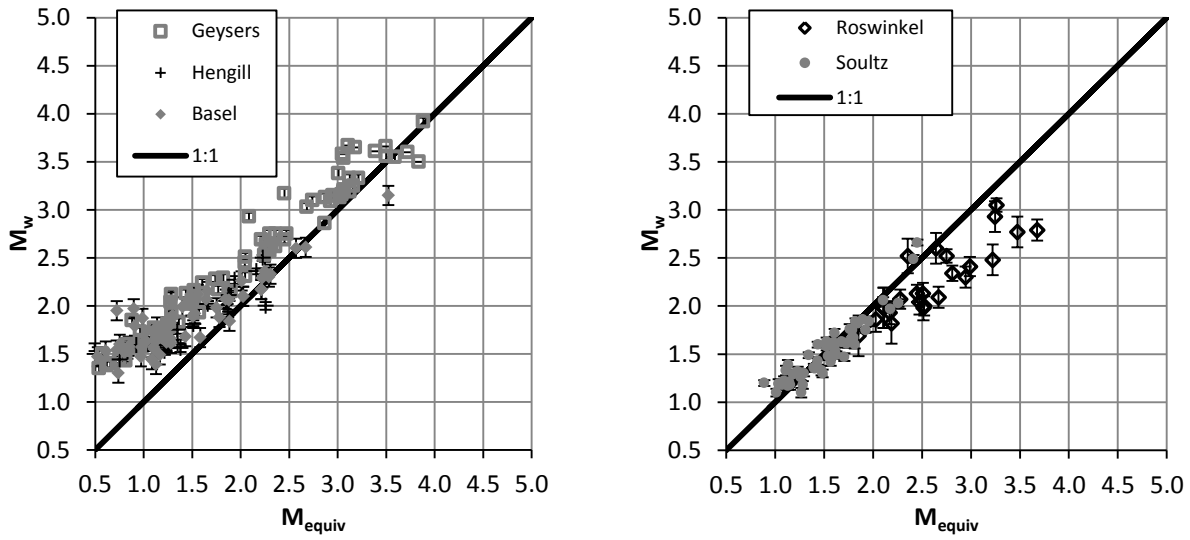

Figure 9: Comparison of common M_{equiv} versus inverted M_w for all datasets in the study. (a) Geysers, Hengill and Basel events. (b) Roswinkel and Soltz events.

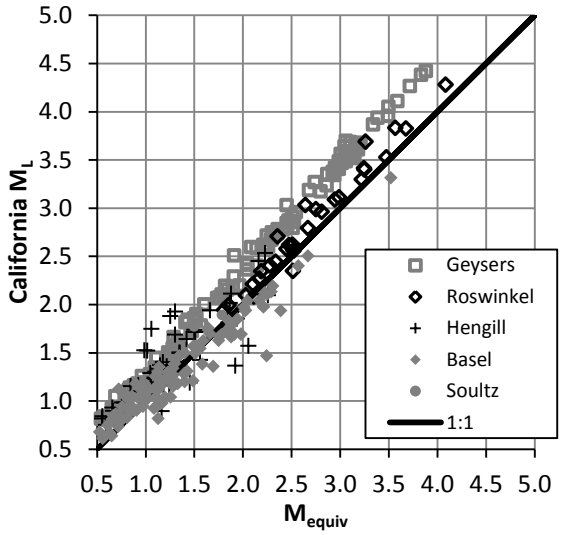

Figure 10: Comparison of M_L using the Southern California attenuation, with M_{equiv}.